HHS Public Access

Author manuscript

Xenobiotica. Author manuscript; available in PMC 2020 October 01.

Published in final edited form as:

Xenobiotica. 2019 October ; 49(10): 1192–1201. doi:10.1080/00498254.2018.1539278.

Antiretroviral Concentrations and Surrogate Measures of Efficacy in the Brain Tissue and CSF of Preclinical Species

Nithya Srinivas[a], **Elias P Rosen**[a], **William M Gilliland Jr.**[a], **Martina Kovarova**[b], **Leila Remling-Mulder**[c], **Gabriela De La Cruz**[b], **Nicole White**[a], **Lourdes Adamson**[d], **Amanda P Schauer**[a], **Craig Sykes**[a], **Paul Luciw**[d], **J. Victor Garcia**[b], **Ramesh Akkina**[c], and **Angela DM Kashuba**[a,*]

[a]Eshelman School of Pharmacy, University of North Carolina at Chapel Hill, Chapel Hill, USA;

[b]School of Medicine, University of North Carolina at Chapel Hill, Chapel Hill, USA;

[c]School of Medicine, Colorado State University, Fort Collins, USA;

[d]School of Medicine, University of California at Davis, Davis, USA

Abstract

1. Antiretroviral concentrations in cerebrospinal fluid (CSF) are used as surrogate for brain tissue, although sparse data support this. We quantified antiretrovirals in brain tissue across preclinical models, compared them to CSF, and calculated 90% inhibitory quotients (IQ_{90}) for nonhuman primate (NHP) brain tissue. Spatial distribution of efavirenz was performed by mass-spectrometry imaging (MSI).

2. HIV or RT-SHIV-infected and uninfected animals from two humanized mouse models (hemopoietic-stem cell/RAG2-, n=36; bone marrow-liver-thymus/BLT, n=13) and an NHP model (rhesus macaque, n=18) were dosed with six antiretrovirals. Brain tissue, CSF (NHPs) and plasma were collected at necropsy. Drug concentrations were measured by LC-MS/MS. Rapid equilibrium dialysis determined protein binding in NHP brain.

3. Brain tissue penetration of most antiretrovirals were >10-fold lower ($p<0.02$) in humanized mice than NHPs. NHP CSF concentrations were >13-fold lower ($p<0.02$) than brain tissue with poor agreement except for efavirenz ($r=0.91$, $p=0.001$). Despite 97% brain tissue protein binding, efavirenz achieved $IQ_{90}>1$ in all animals and 2-fold greater white versus grey matter concentration.

4. Brain tissue penetration varied across animal models for all antiretrovirals except raltegravir, and extrapolating brain tissue concentrations between models should be avoided. With the exception of efavirenz, CSF is not a surrogate for brain tissue concentrations.

Keywords

antiretrovirals; brain tissue; cerebrospinal fluid; efavirenz; HIV; mass spectrometry imaging; protein binding

*Corresponding Author: Angela D. M. Kashuba, BScPhm, Pharm.D., DABCP, 1094 Genetic Medicine Building, CB# 7361, 120 Mason Farm Road, UNC Eshelman School of Pharmacy, Division of Pharmacotherapy and Experimental Therapeutics, University of North Carolina at Chapel Hill, North Carolina, NC 27599, Tel (919) 966-9998 Fax (919) 962-0644, akashuba@unc.edu.

I. Introduction

HIV invades the central nervous system (CNS) early after infection. HIV RNA can be detected in the cerebrospinal fluid (CSF) of acutely infected patients eight days after HIV exposure (Valcour et al. 2012), and may be detected in the CSF even when undetectable in the plasma (Edén et al. 2010; Farhadian et al. 2017). In the brain, HIV replication occurs in long lived cells such as macrophages (Joseph et al. 2014), and the resulting immune activation is hypothesized to cause neuronal cell death and decline in neurological functioning (New et al. 1998; Zayyad & Spudich 2015). Before combination antiretroviral (ARV) therapy, almost 60% of patients with AIDS developed HIV associated dementia (HAD) (Ances & Ellis 2007). Currently, the prevalence of HAD has been reduced to 5%, although milder forms of neurocognitive impairment remain highly prevalent at 20–50% (Marra 2015). This may be related to ARV penetration into the CNS (Letendre 2011). While our understanding of ARV exposure/response in the CSF has greatly improved in the past decade, some key knowledge gaps still exist.

The first critical knowledge gap is the extent of ARV penetration into the brain tissue and agreement between CSF and brain tissue concentrations of ARVs. The brain is the relevant target site for HIV replication in the CNS, however, a paucity of information exists on ARV concentrations achieved in the brain tissue. Furthermore, while CSF concentrations are often considered as a surrogate for brain tissue exposure, little data support this for ARVs. For several classes of drugs acting in the CNS, CSF concentrations are either much lower than, or not predictive of, brain tissue concentrations (Liu et al. 2006; Rambeck et al. 2006). This may also be the case for ARVs due to their affinity for the drug uptake and efflux transporters at the blood-brain barrier (BBB) and the blood-CSF barrier (B-CSF-B). Active transport of ARVs along the BBB and B-CSF-B disturbs the equilibrium of passive protein-unbound drug movement (Smith et al. 2010), which may result in different relationships between plasma, CSF and brain tissue concentrations for different ARVs.

The second critical gap is related to defining an appropriate efficacy target for drug exposure in the CNS. An efficacy target that is commonly employed is the drug concentration required to inhibit HIV viral replication by 50% (IC_{50}). While achieving drug concentration $>IC_{50}$ has been generally considered optimal in the CSF (Best et al. 2011; Croteau et al. 2010), having coverage at IC_{50} concentrations may not be enough to avoid the onset of resistance mutations (Calcagno et al. 2015). In a recent analysis by Calcagno (2015), inhibitory quotients (IQ) were calculated for commonly used ARV regimens in the CSF by using a standardized wild-type IC_{95} for HIV clinical isolates (Acosta et al. 2012). The investigators were able to demonstrate the utility of this measurement in optimizing CNS-penetrating ARV regimens by showing that an $IQ_{95}>1$ was associated with better viral control in the CSF. While such an approach could provide a standardized drug efficacy target across studies, the wild-type IC_{95} estimates utilized in this analysis were corrected for protein binding in the plasma and not the CSF. Since drugs usually exhibit a higher extent of protein binding in the plasma compared to the CSF (Nguyen et al. 2013; Avery et al. 2013), it is likely that some of the final IQ estimates may have been underestimated. Furthermore, these values have not been determined for brain tissue.

Since it is not practical to obtain robust human brain tissue pharmacokinetic (PK) data, animal models can be used to address the knowledge gaps detailed above. In this work, we measure the penetration of ARVs across commonly used HIV preclinical models – two humanized mouse models and one nonhuman primate (NHP) model (Denton & Garcia 2009; Hatziioannou & Evans 2012). In the NHPs, we evaluate the agreement between total ARV concentrations in the brain tissue and CSF and measure unbound ARV brain tissue concentrations in order to calculate IQ_{90} estimates. To provide a measure of spatial brain tissue distribution, we further investigate efavirenz (EFV). By using mass-spectrometry imaging (MSI) combined with immunohistochemistry, we determine the distribution pattern of EFV in the NHP brain, and colocalization with relevant HIV target cells.

II. Materials and Methods

Tissue collection from animal models

This analysis utilized three commonly used animal models: two species of humanized mice (human stem cell hemopoietic/Rag 2- [hu-HSC-Rag, n=36] and bone marrow-liver-thymus [BLT, n=13]) and one species of NHP (rhesus macaques [n=18]). All of the humanized mice were female, while six (33.3%) of the NHPs were female. Approximately one-half of the animals were left uninfected or were infected with $HIV_{BAL\text{-}D7}$ (hu-HSC-Rag mice), HIV_{JRcsf} (BLT mice) or RT-SHIV (NHPs) (North et al. 2005; North et al. 2010), for four weeks. All animals were dosed with combinations of six ARVS representing five ARV classes: tenofovir (TFV), emtricitabine (FTC), EFV, raltegravir (RAL), maraviroc (MVC) and atazanavir (ATZ). BLT mice were not dosed with EFV due to prior toxicity concerns but were dosed with a combination of TFV/FTC/RAL/MVC/ATZ (six uninfected and seven infected animals). Hu-HSC-RAG were divided into three groups and dosed with EFV only (six uninfected and six infected animals), ATZ only (six uninfected and six infected animals) or TFV/FTC/RAL/MVC (six uninfected and six infected animals). In the NHPs, animals were dosed with TFV/FTC/EFV/RAL (four uninfected and five infected animals) or TFV/FTC/MVC/ATZ (four uninfected and five infected animals). The dosage regimens selected (Supplementary Table 1) were based on doses commonly used in the animal models for virologic efficacy (Neff et al. 2010; Denton et al. 2010; Shytaj et al. 2012) and the specific regimens were chosen either for site-specific practical considerations (humanized mice) or to minimize the potential for drug-drug interactions (NHPs). ARVs were dosed for ten days to achieve PK steady state conditions based on the half-lives of these drugs. Necropsy was scheduled one day later. Detailed methods on the animal studies, including dosing regimens, are provided in the supplementary material. For the NHPs, plasma, CSF, and brain tissue (frontal lobe, cerebellum, basal ganglia, and parietal lobe) were collected at necropsy. These regions were chosen to investigate cortical (frontal and parietal lobes) and sub-cortical (cerebellum and basal ganglia) brain regions, to investigate morphologically different areas, and to select those areas that showed more extensive involvement in HIV-injury. For the humanized mice, plasma and whole brain tissue were collected. Animal studies were performed in concordance with locally approved institutional animal care and use committee (IACUC) protocols from the University of North Carolina at Chapel Hill (protocol 15–168), Colorado State University (protocol 16–6998A) and the University of California at Davis (protocol 18345).

Sample analysis for parent drug

Sample analysis has been described in detail elsewhere (Thompson et al. 2017). Briefly, plasma and CSF were extracted by protein precipitation using stable, isotopically labelled internal standards. The extracts were analyzed on a Shimadzu HPLC system with a Waters Atlantis T3 (50 mm × 2.1 mm, 3 μm particle size) column, with an API 5000 mass spectrometer (SCIEX, Framingham, MA) detector equipped with a TurboIonSpray interface. The lower limit of quantification (LLOQ) was 1 ng/mL. The inter- and intra-day precision and accuracy of the assay was within 15%.

Brain tissue samples were homogenized in 1 mL of 70:30 acetonitrile:1 mM ammonium phosphate (pH 7.4) and then extracted by protein precipitation with stable, isotopically labelled internal standards. TFV and FTC were analyzed by the method described for fluids while ATZ, EFV, MVC, and RAL were separated using an Agilent Pursuit XRs 3 Diphenyl (50 mm × 2 mm, 3 μm particle size) HPLC column. The LLOQs of the brain tissue homogenate were 0.002 ng/mL (FTC and MVC), 0.005 ng/mL (ATZ, EFV, and RAL), and 0.01 ng/mL (TFV). These concentrations in ng/mL were converted to ng/g using a density of 1.06 g/m^3. The intracellular active metabolites of TFV (tenofovir diphosphate: TFV-dp) and FTC (emtricitabine triphosphate: FTC-tp) were also quantified in the brain tissue. TFV-dp and FTC-tp were extracted by homogenizing the tissue with 70:30 acetonitrile:1 mM ammonium phosphate (pH 7.4). An aliquot of the resulting homogenate was mixed with acetonitrile containing an isotopically-labelled internal standard, 13C5-TFV-dp, (Moravek Biochemicals, Brea, CA). The extracts were evaporated to dryness, reconstituted with 1 mM ammonium phosphate (pH 7.4), and transferred to a 96-well plate for analysis. TFV-dp and FTC-tp were analyzed using anion exchange chromatography on a Thermo BioBasic AX (50 × 2.1 mm, 5 μm particle size) analytical column (Waters, Milford, MA) followed by detection under positive ion electrospray conditions. Data were collected using an AB Sciex API-5000 triple quadrupole mass spectrometer. The dynamic range was 0.300–300 ng/mL homogenate (rhesus macaques) and 0.0200 – 300 ng/mL homogenate (humanized mice) for both TFV-dp and FTC-tp.

Determination of protein binding in the NHP brain tissue

The protein binding of EFV, RAL, MVC, and ATZ in the brain tissue was determined by rapid equilibrium dialysis (RED). Briefly, 5–10 mg of frontal cortex brain tissue samples were homogenized in Precelly's tubes and incubated at 37°C for 18 hours in rapid equilibrium dialysis cartridges (Thermo Scientific, Pittsburg, PA). The samples subsequently underwent liquid-liquid extraction with methyl tert-butyl ether (MTBE) (Fisher Scientific, Norcross, GA, USA) using an Agilent 1200 series HPLC System and an Agilent 1100 MSD (Agilent Technologies, New Castle, DE) in positive ESI mode. Analytes were then separated on an Agilent Zorbax Eclipse XDB-C8 (3.0 mm × 50 mm, 1.8 m) column. Assay sensitivity was 2 ng/ml and inter- and intra-day assay precision was within 15%. The median fraction unbound value was used to determine the unbound ARV concentrations across all NHP brain tissue samples.

Calculation of 90% Inhibitory Quotients in NHP brain tissue

IQ_{90} was calculated as a surrogate measure of ARV efficacy in the brain tissue using the protein-unbound brain tissue concentrations and the protein-unbound IC_{90} for the RT-SHIV strain of virus, when available. Since the RT-SHIV viral strain has the reverse transcriptase (RT) enzyme from HIV-1 clinical isolates, the IC_{90} values of ARV classes targeting this enzyme: nucleoside reverse transcriptase inhibitors (NRTIs) and non-nucleoside reverse transcriptase inhibitors (NNRTIs) were taken from the values for HIV-1 clinical isolates from various sources (Acosta et al. 2012; Van Rompay et al. 1996; Mathez et al. 1993). MVC IC_{90} values for RT-SHIV were available from Pal (2012) and RAL IC_{90} values for RT-SHIV were available from Hassounah (2014). The IC_{90} value of ATZ against RT-SHIV (12,750 ng/g) was calculated from concentration-response data provided by Z. Ambrose (personal communication, September 18th, 2018). All values were corrected for protein binding as described by Yilmaz (2012). The formula for ARV IQ_{90} in brain tissue is given by equation 1.

$$IQ_{90} = \frac{ARV\ protein-unbound\ concentration\ in\ the\ brain\ tissue}{Protein-free\ wild-type\ IC90\ of\ RT-SHIV} \quad (1)$$

Mass spectrometry imaging

We chose to investigate EFV concentrations by MSI due to its accumulation in brain tissue (Thompson et al. 2015) and its well-known clinical toxicity profile. Methods for the Infrared Matrix-Assisted Laser Desorption Electrospray Ionization (IR-MALDESI) MSI analysis have been published previously (Barry et al. 2014; Thompson et al. 2015). Briefly, 10 μm thick frozen slices of discrete tissue regions (NHPs) or whole brain (humanized mice) were thaw-mounted onto a glass slide, covered with an ice layer and ablated with 2 mid-IR laser pulses with a 100 μm spot-to-spot distance. Ablated molecules were ionized by electrospray and sampled into a Thermo Fisher Scientific Q Exactive mass spectrometer (Bremen, Germany) for analysis. Raw data from each volumetric pixel (voxel) were converted to the mzXML format and then imzML format to evaluate using MSiReader (Robichaud et al. 2013). Quantification of EFV concentration was achieved by spotting calibration standards of known concentration onto a non-dosed brain tissue slice (Bioreclamation IVT, Baltimore, MD). The resulting ng/slice concentrations were converted to ng/g using the area of each slice, tissue thickness, and a density of 1.06 g/mL. The limit of detection for EFV was 123 fg/voxel (100 μm × 100 μm × 10 μm), or 0.1 ng/g tissue.

Drug Colocalization to HIV target cells in the brain tissue

Dual immunofluorescence staining was performed on frozen humanized mouse and NHP brain tissue sections for CD3/CD4 (CD4+ T-cells) and CD45/CD11b (microglial cells) in the Bond fully-automated slide staining system (Leica Microsystems) using the Bond Polymer Refine Detection kit (DS9800). The slides were brought to room temperature for 15 minutes and were then fixed in 10% neutral buffered formalin for 15 minutes. Following this procedure, slides were placed in Bond wash solution (AR9590) and antigen retrieval was done at 100°C in Bond-epitope retrieval solution 2 pH 9.0 (AR9640) for ten minutes.

Co-registration of EFV and target cell distribution images were performed using the Matlab v. R2015a Image Processing Toolbox (Mathworks, Natick, MA). Co-registration of images was performed on the cholesterol MSI image using a background DAPI IF stain as a reference to ensure that the MSI and IF images were aligned appropriately before co-localization. The transformed ARV images were overlaid with the variable of interest (CD4, or CD11b) to generate a fused image containing both the ARV (in red) and the cellular variable of interest (in green). After image overlay was performed, the fractional coverage of the sum of the total cellular area which contained detectable drug concentration and drug concentration >IC_{50} and IC_{90} target values were calculated.

Statistical Analysis

Since the same mg/kg ARV dose was not given to all species, ARV concentrations were normalized to the systemic concentrations in plasma to give either a CSF:plasma ratio or a brain tissue:plasma ratio, in order to make inter-species comparisons of drug penetration. Comparisons between species, and brain tissue and CSF compartments were made using the Kruskal-Wallis test ($p<0.01$ was considered significant). The Spearman rank-order correlation test was used to determine the relationship between the ARV concentrations in brain tissue and CSF. Data were analyzed using SigmaPlot 13.0 (Systat Software Inc., San Jose, CA) and are presented as median (range) unless otherwise noted.

III. Results

ARV penetration into the brain tissue varied markedly across humanized mice and nonhuman primates except for RAL

Brain tissue concentrations from 36 hu-HSC-RAG mice, 13 BLT mice, and 17 NHPs were available for the final inter-species comparison. By LC-MS/MS analysis, ARV concentrations in the four brain regions of the NHPs did not differ (Supplementary Figure 1; **$p>0.08$**). Therefore, these concentrations were combined for one measure of brain tissue concentration per NHP.

Figure 1 shows the brain tissue:plasma penetration ratio of ARVs, and concentration of active metabolites in the brain tissue across the three preclinical species. ARV penetration ratios into brain tissue of humanized mice ranged from 0.001 (TFV and FTC) to 100 (ATZ) (Figure 1a). Generally, ARV penetration was higher into the brain tissue of BLT mice compared to the hu-HSC-RAG mice. For example, brain tissue penetration was 5-fold higher for MVC ($p=0.002$) and 3- and 5-fold higher, for TFV and FTC ($p>0.15$) respectively in the BLT mice compared to the hu-HSC-RAG.

ARV brain tissue penetration in the NHPs was 10- to 100-fold higher than the BLT mice ($p<0.006$), and 5- to 100-fold higher than the hu-HSC-RAG mice ($p<0.02$) for all ARVs except for RAL. For most ARVs, this result was due to lower ARV concentrations in the brain tissue and plasma of both humanized mouse models (Supplementary Table 2). However, in the case of TFV and FTC, the low brain tissue penetration in the two humanized mouse models was a result of lower brain tissue concentrations and higher plasma concentrations in the mice compared to NHPs. The brain tissue:plasma ratio of RAL

(median of 0.11–0.12; p=0.6) was preserved across all three species while the brain tissue:plasma penetration ratio of MVC (median of 1; p=1.0) was similar in the BLT mice and NHPs (Figure 1a **and** supplementary table 2).

The active metabolite of TFV, TFV-dp, was quantifiable in all brain tissue samples, with concentrations ranging from 851 to 179,000 fmol/g of tissue (Figure 1b). Median brain tissue concentrations of TFV-dp were 10-fold higher in the hu-HSC-RAG mice (14700 fmol/g) compared to the BLT mice (1440 fmol/g), despite TFV concentrations being lower in the hu-HSC-RAG mice, though this did not reach statistical significance (p=0.29). TFV-dp concentration in the NHP brain was 34,800 (15,000–179,000) fmol/g. Due to the low concentration of FTC in the brain tissue for both the humanized mouse models (3.31 ng/g [0.14 ng/g to 29.1 ng/g] and nonhuman primates (26.3 ng/g [2.0 ng/g to 69.3 ng/g]), its active metabolite FTC-tp was not quantifiable across all three animal models.

As an exploratory objective, we evaluated whether infection status and sex influenced ARV penetration into the brain tissue in NHPs. We found no significant differences for any of the ARVs on the basis of these factors (p>1.0).

Except for EFV, ARV concentrations in brain tissue were significantly higher than the CSF and poorly correlated

In Figure 2, total ARV concentrations in the CSF and brain tissue of NHPs are shown. EFV reached the highest concentration in the brain tissue (775 [240–1982] ng/g) which was 9- to 36-fold higher than other ARVs, where median concentrations were <100 ng/g (Figure 2a **and** Supplementary Table 2). The lowest brain tissue concentrations were found for FTC (26.3 [2.0–69.2] ng/g) and RAL (21.8 [11.5–265] ng/g). ARV concentrations in the CSF were consistently lower (by 13- to 1,150-fold; p<0.001) than the brain tissue. Only the total CSF concentrations of EFV strongly correlated with total brain tissue concentrations (r=0.91, p<0.001). No correlation between CSF and brain tissue concentration was found for the other ARVs (r<0.5, p >0.15) (Figure 2b).

Despite high protein binding in brain tissue of nonhuman primates, EFV maintained an IQ_{90} >1

Protein binding in the brain tissue for EFV was 97% (91%, 98%), whereas it was lower for ATZ (24% [0%, 39%]), and negligible for MVC (3%, [0%, 19%]). Due to low concentrations of RAL in brain tissue, the fraction unbound could only be estimated for one of the samples (24%).

The IQ_{90} calculated using the unbound brain tissue drug concentration (EFV, MVC, ATZ, and RAL) and protein-free IC_{90} values, are shown in the open circles in Figure 3. Only EFV consistently had an IQ_{90} >1 in all of the animals. One animal showed a RAL IQ_{90} of 1.1 while another animal showed a TFV-dp IQ_{90} of 1.1. For MVC, ATZ, TFV, and FTC, none of the animals had an IQ_{90} >1.

Mass-spectrometry imaging demonstrated heterogeneous distribution of EFV in brain tissue

The MSI results for NHPs in Figure 4 show response for the endogenous markers cholesterol (Figure 4, **left-pane**), which was used to delineate regions of white matter (WM) and grey matter (GM), and heme (Figure 4, **middle-pane**), which was used as a surrogate for blood contamination in the brain tissue samples. EFV distribution (Figure 4, **right-pane**) was masked based on the heme distribution in order to show the EFV response that did not colocalize with heme. EFV distribution was visualized in only one hu-HSC-RAG mouse, which had the highest EFV brain tissue concentration measured by LC-MS/MS (1,400 ng/g) (Figure 4a). In this animal, drug distribution was relatively homogeneous across the brain structures and heme distribution accounted for 30% of the summed EFV MSI response across the tissue. EFV was not detected in the other mice, where concentrations were <35 ng/g. In the NHPs, EFV was detected in all tissue samples (and LC-MS/MS concentrations were all >150 ng/g). In the uninfected animals (Figure 4b), EFV concentrations were 1.1- to 3-fold higher in the WM relative to the GM. The variability (as defined by CV%) of concentration/voxel in the uninfected animals was approximately 85% in the GM and 78% in the WM. Compared to the uninfected NHPs, RT-SHIV infected animals showed 86% lower EFV concentration across brain tissue (Figure 4c), and no morphological differences in EFV distribution pattern were evident. The variability (CV%) of concentration/voxel in the infected NHPs was similar to the uninfected NHPs; 77% in the GM and 83% in the WM. The heme response was negligible in the uninfected and SHIV-infected NHPS and accounted for only 1% of the summed EFV MSI response across the tissue.

EFV showed low colocalization with HIV target cells

In Figure 5, the overlay of CD11b cells is shown with EFV drug exposure in the cerebellum of an uninfected NHP (Figure 5a) and a SHIV-infected NHP (Figure 5b). For uninfected animals, the fraction of total CD11b or CD4+ T-cell cellular area with detectable EFV concentrations ranged from 50–80%. For the infected animals, the fractional coverage of cells containing detectable EFV was similar, ranging from 45–70%. However, the fractional coverage of CD4 and CD11b cells that contained total concentration of EFV above an IC_{50} target of 2 ng/g was only ~3% regardless of infection status. No cells colocalized with EFV concentrations > IC_{90} target.

IV. Discussion

In this analysis, we present a comprehensive overview of brain tissue concentrations of ARVs across three commonly used HIV preclinical models. We show that ARV brain tissue penetration by LC-MS/MS is highly variable between the ARVs (50–150%), and between the animal models for a given ARV. This variability is similar to, or higher than, the variability found with human CSF ARV concentrations (~35%) (Calcagno et al. 2015).

Comparing drug exposure between the species, brain tissue penetration rank order distinctively increased from hu-HSC-RAG mice to BLT mice to NHPs for TFV and FTC. For EFV, MVC and ATZ, brain tissue penetration was higher for NHPs than humanized mice. RAL penetration was similar between the species. While the exact reason for this is

unclear, drug interactions and underlying physicochemical properties may play a role. For example, RAL is a substrate of both P-gp and BCRP. While our group and others have shown higher BCRP concentration in NHPs compared to humanized mice (Ito et al. 2011; Thompson et al. 2017), RAL was co-administered with EFV in the NHPs which inhibits BCRP (Weiss et al. 2007). The resulting interaction in the NHPs may have led to equivalent brain tissue penetration across all three species. Similarly, the greater brain tissue:plasma penetration of TFV, FTC, and MVC in the BLT mice relative to the hu-HSC-RAG mice may be due to co-administration of these ARVs with ATZ in the BLT model, which inhibits drug efflux by P-gp, BCRP, and MRP1 (Griffin et al. 2011). While we were not able to avoid drug-drug interactions due to the limited number of animals, such interactions are also clinically unavoidable since multiple drugs are used in HIV treatment regimens. In such cases, preclinical models can be used to test how different ARV combinations may affect tissue distribution.

In this study, CSF ARV concentrations in NHPs approximated human concentrations as reported by Calcagno (2014). FTC was the one exception, where CSF concentrations were approximately 3-fold lower in NHPs. While there are fewer human brain tissue studies to compare to our preclinical models, one recent study by Nicol (2018) provides some insights. Three African men with AIDS taking EFV and TFV had brain tissue concentrations measured post-mortem. The median concentrations of EFV and TFV were 900 ng/g and 80 ng/g which agree with the values we report here in the NHPs (775 ng/g and 65 ng/g, respectively).

With the exception of EFV, we found that ARV CSF concentrations were consistently lower than, and not predictive of, brain tissue concentrations. This was shown across all classes of drugs, irrespective of drug lipophilicity, pKa, drug transporter affinity, or other physicochemical properties, and agrees with the literature for several classes of CNS-acting drugs (Liu et al. 2006; Rambeck et al. 2006). For low permeability compounds such as TFV and MVC (both ARVs are BCS class III), CSF concentrations may have underpredicted brain tissue concentrations due to the fast recycling rate of the CSF that acts like a ‘sink’ to clear drug (Shen et al. 2004). For other ARVs that have higher permeability, underlying interactions between ARVs and drug transporters might also play a role in the discrepancy between drug concentration measurements. For example, FTC is a highly permeable drug (BCS class I) and is a substrate of MRP1 (Bousquet et al. 2008), an efflux transporter that is localized on the basolateral membrane of the B-CSF-B. MRP1 effluxes drug-substrates out in the direction of CSF to blood (Wijnholds et al. 2000; Strazielle & Ghersi-Egea 2015) at the B-CSF-B but is not found on the BBB (Strazielle & Ghersi-Egea 2015). Thus, the presence of MRP1 on the B-CSF-B but not on the BBB could result in lower FTC concentrations in the CSF relative to the brain tissue. For the remaining ARVs: EFV, RAL, and ATZ, which are highly permeable (BCS class I or class II) and substrates of either P-gp or BCRP, our results may appear to contradict conventional understanding, since P-gp and BCRP are both localized on the apical membrane of the BBB (direction of drug-efflux is brain to blood) and the B-CSF-B (direction of drug-efflux is blood to CSF) (Strazielle & Ghersi-Egea 2015). However, many of these ARVs (FTC, EFV, MVC, and ATZ) are also inhibitors of P-gp and BCRP (Alam et al. 2016). As previously discussed, co-administration of multiple ARVs may have resulted in significant inhibition of the function of P-gp and

BCRP and accumulation of ARVs in the brain tissue relative to the CSF. These data suggest that deriving concentration-efficacy relationships in the CNS using only CSF concentrations may be inaccurate.

This is the first study to define ARV IQ_{90} in the brain tissue using protein-unbound brain tissue concentrations. We chose to calculate IQ values since they have previously demonstrated utility in studying the relationship between drug exposure and efficacy (Hoefnagel et al. 2005; Winston & Khoo 2008). Targeting IQ_{90}>1 in plasma has been associated with improvement in virologic control and clinical outcomes (Hoefnagel et al. 2005; Winston & Khoo 2008). Recent work by Calcagno (2015) suggested that the CSF IQ_{95} may guide the rational selection of CNS-targeted ARV regimens. In order to derive the IQ_{90} in the brain tissue, we measured the unbound tissue concentrations for EFV, RAL, MVC, and ATZ. Since TFV and FTC protein binding in plasma is <10%, we used the total concentrations in brain tissue for their IQ_{90} estimation The extent of drug binding in the brain tissue was low (0–24%) for all ARVs except EFV (91–99%). The degree of brain tissue binding we measured here for all ARVs was lower than the blood plasma protein binding. For example, ATZ has been shown to be highly bound in the blood plasma (86%) (Boffito et al. 2003), however the median binding of ATZ in the brain tissue was only 24%. Similarly, MVC has been shown to be moderately bound in the blood plasma (~76%) (MacArthur et al. 2008), however, the binding of MVC to the brain tissue was negligible (<3%). These results can be explained by the very low concentration of drug binding proteins in the brain tissue relative to the plasma. For example, plasma albumin concentrations are 35–50 g/L whereas brain tissue albumin concentrations are <1 mg/L (Srinivas et al. 2018). The relatively high protein binding of EFV in the brain (97%) tissue, comparable to the plasma (99.5%) (Boffito et al. 2003), may be due to the high lipophilicity of EFV (logP=4.6) and the binding affinity of EFV for CYP46A1 (cholesterol hydroxylase), an enzyme localized to the endoplasmic reticulum of neurons (Anderson et al. 2016; Mast et al. 2014).

Our finding that drug concentrations in the brain tissue are >75% unbound for most ARVs is important to understand drug efficacy and toxicity. For example, ATZ has been shown to cause neuronal toxicity, both in pig-tail macaques (with the same dosage regimen of ATZ used in this study), as well as in an in-vitro system of human cells (Robertson et al. 2012). The unbound brain tissue concentrations of ATZ measured in our study (38 ng/g to 418 ng/g) were at least two-fold higher than the total ATZ concentrations that caused neuronal toxicity in the human in-vitro system, potentially explaining the macaque toxicity finding. Our data are the first that can be used to make this connection since previous analyses relied on CSF concentrations of ATZ which are low (5–21 ng/mL) (Best et al. 2009). High concentrations in the human brain tissue may also explain the reported clinical cases of CNS toxicity due to ATZ (Martina 2013).

We also demonstrated that for most ARVs, the IQ_{90} was <1 in all of the animals. For RAL, the IQ_{90} in the one animal where we could measure unbound brain tissue concentration was 0.07. Even when using total brain tissue concentrations, the IQ_{90} of RAL was <1 for six of the remaining seven animals. We also show that despite a high degree of protein binding in

the brain tissue, EFV still achieved an IQ_{90} of >1, in all eight animals. This suggests that by the IQ method, free EFV brain tissue concentrations may be high enough to achieve efficacy.

The results above were based on tissue homogenate LC-MS/MS analysis. However, the results of our MSI analysis indicated that there was heterogeneity in EFV distribution into the brain tissue that led to a different estimation of surrogate efficacy. In uninfected NHPs, EFV had a relatively heterogeneous distribution across brain tissue, accumulating up to 3-fold higher in the cerebellar WM versus GM. This widespread EFV distribution may be a function of neuronal binding to CYP46A1(Anderson et al. 2016; Mast et al. 2014), as described above. In the case of infected NHPs, the brain tissue concentrations were 7-fold lower, which made it more difficult to detect regional differences in drug localization. Interestingly, despite all animals having EFV concentrations $>IC_{90}$ by LC-MS/MS analysis, none of the areas (particularly GM) where we detected microglial cells or CD4+ T-cells (targets for HIV infection/replication) contained EFV at concentrations $>IC_{90}$ by MSI analysis. Rather, preferential accumulation of EFV was in the WM. These preliminary results indicate the potential for suboptimal coverage of active EFV within the brain tissue despite high IQs as measured by tissue homogenate. Future experiments imaging viral replication in the CNS along with drug concentrations should be performed to understand the clinical implications of these findings.

There were a few limitations to this investigation. Sex differences in the plasma PK of laboratory animals have been observed with several classes of anti-infective and CNS-acting drugs (Czerniak 2001). Although we were unable to secure male humanized mice for this study, we evaluated the CNS distribution of ARVs in male and female NHPs and did not find any substantive differences in CSF or brain tissue concentrations on the basis of sex. Another limitation of this study is the missing information on IC_{90} values against the RT-SHIV strain of virus for several of the ARVs in our analysis. As mentioned earlier, in case of the NRTIs and NNRTIs, using the IC_{90} for the clinical HIV-1 isolates was a reasonable estimate (Witrouw et al. 2004). Finally, the IC_{90} values against RT-SHIV were 20-fold (RAL), 100-fold (MVC), and 1,000-fold (ATZ) higher than against clinical HIV-1 isolates. If unbound exposures in the human brain tissue approximate the NHP exposures, MVC, ATZ, and RAL would achieve $IQ_{90} \geq 1$ in the human brain.

From the results presented in this study, ARV penetration into the brain tissue relative to plasma was 10- to 100-fold higher in the NHPs compared to the humanized mice and was only preserved across all three species for RAL. In the NHPs, the brain tissue concentrations of ARVs were 10- to 1000-times higher than in the CSF, and could not be estimated by CSF concentrations for most ARVs except for EFV. Because of these findings, the CSF may not be a reliable surrogate for brain tissue concentrations. Except for EFV, all ARVs were >75% unbound in the brain tissue but only EFV had protein-unbound concentrations in the brain tissue $>IQ_{90}$ in all the animals. However, our IR MALDESI investigations found that EFV poorly colocalized with HIV-target cells in the brain as a result of preferential accumulation in the WM. These results show that despite a high concentration of free drug, lack of adequate EFV coverage at the target cells of interest may contribute to HIV persistence in the brain (Mukerji et al. 2018) and should be investigated further.

Supplementary Material

Refer to Web version on PubMed Central for supplementary material.

Acknowledgements:

1. The authors would like to express our gratitude to Drs. Thibault Mesplède and Said A. Hassounah for providing IC_{90} values for raltegravir against RT-SHIV isolate

2. The authors would like to Dr. Zandrea Ambrose for providing IC_{90} values for atazanavir against RT-SHIV isolate

Declaration of interest statement:

This research was supported by the NIH under the grant nos. RO1 AI111891, RO1 MH108179 and in part by an instrument grant S10 RR024595. This research is supported in part by the UNC Center for AIDS Research under the grant no. P30 AI50410. Nonhuman primate studies were supported in part by the Base Grant to the California National Primate Research Center P51 OD011107. The authors have no conflict of interests to declare.

Sources of Funding:

This work was supported by the NIH under Grants RO1 AI111891, RO1 MH108179 and S10 RR024595; UNC Centre for AIDS Research under Grant P30 AI50410; and California National Primate Research Center under Grant P51 OD011107. NS was supported by the Royster Society of Fellows

References:

Acosta EP, Limoli KL, Trinh L, Parkin NT, King JR, Weidler JM, Ofotokun I, & Petropoulos CJ (2012). Novel method to assess antiretroviral target trough concentrations using in vitro susceptibility data. Antimicrobial Agents and Chemotherapy, 56(11), 5938–45. [PubMed: 22964257]

Alam C, Whyte-Allman SK, Omeragic A, & Bendayan R (2016). Role and modulation of drug transporters in HIV-1 therapy. Advanced Drug Delivery Reviews, 103, 121–43. [PubMed: 27181050]

Ances BM, & Ellis RJ, (2007). Dementia and neurocognitive disorders due to HIV-1 infection. Seminars in Neurology, 27(1), 86–92. [PubMed: 17226745]

Anderson KW, Mast N, Hudgens JW, Lin JB, Turko IV, & Pikuleva IA, (2016). Mapping of the allosteric site in cholesterol hydroxylase CYP46A1 for efavirenz, a drug that stimulates enzyme activity. Journal of Biological Chemistry, 291(22), 11876–86. [PubMed: 27056331]

Avery LB, Sacktor N, McArthur JC, & Hendrix CW, (2013). Protein-free efavirenz concentrations in cerebrospinal fluid and blood plasma are equivalent: Applying the law of mass action to predict protein-free drug concentration. Antimicrobial Agents and Chemotherapy, 57(3), 1409–14. [PubMed: 23295919]

Barry JA, Robichaud G, Bokhart MT, Thompson C, Sykes C, Kashuba AD, & Muddiman DC, (2014). Mapping antiretroviral drugs in tissue by IR-MALDESI MSI coupled to the Q Exactive and comparison with LC-MS/MS SRM assay. Journal of the American Society for Mass Spectrometry, 25(12), 2038–47. [PubMed: 24744212]

Best BM, Letendre SL, Brigid E, Clifford DB, Collier AC, Gelman BB, McArthur JC, McCutchan JA, Simpson DM, Ellis R, Capparelli EV, & Grant I; CHARTER Group, (2009). Low atazanavir concentrations in cerebrospinal fluid. AIDS, 23(1), 83–7. [PubMed: 19050389]

Best BM, Koopmans PP, Letendre SL, Capparelli EV, Rossi SS, Clifford DB, Collier AC, Gelman BB, Mbeo G, McCutchan JA, Simpson DM, Haubrich R, Ellis R, & Grant I; CHARTER Group, (2011). Efavirenz concentrations in CSF exceed IC50 for wild-type HIV. Journal of Antimicrobial Chemotherapy, 66(2), 354–7. [PubMed: 21098541]

Boffito M, Back DJ, Blaschke TF, Rowland M, Bertz RJ, Gerber JG, & Miller V (2003). Protein binding in antiretroviral therapies. AIDS Research and Human Retroviruses, 19(9), 825–35. [PubMed: 14585213]

Bousquet L, Pruvost A, Didier N, Farinotti R, & Mabondzo A (2008). Emtricitabine: inhibitor and substrate of multidrug resistance associated protein. European Journal of Pharmaceutical Sciences, 35(4), 247–56. [PubMed: 18692133]

Calcagno A, Di Perri G, & Bonora S, (2014). Pharmacokinetics and pharmacodynamics of antiretrovirals in the central nervous system. Clinical Pharmacokinetics, 53(10), 891–906. [PubMed: 25200312]

Calcagno A, Simiele M, Alberione MC, Bracchi M, Marinaro L, Ecclesia S, Di Perri G, D'Avolio A, & Bonora S, (2015). Cerebrospinal fluid inhibitory quotients of antiretroviral drugs in HIV-infected patients are associated with compartmental viral control. Clinical Infectious Diseases, 60(2), 311–7. [PubMed: 25281609]

Croteau D, Letendre S, Best BM, Ellis RJ, Breidinger S, Clifford D, Collier A, Gelman B, Marra C, Mbeo C, McCutchan A, Morgello S, Simpson D, Way L, Vaida F, Ueland S, Capparelli E, & Grant I; CHARTER Group, (2010). Total raltegravir concentrations in cerebrospinal fluid exceed the 50-percent inhibitory concentration for wild-type HIV1. Antimicrobial Agents and Chemotherapy, 54(12), 5156–60. [PubMed: 20876368]

Czerniak R, (2001). Gender-based differences in pharmacokinetics in laboratory animal models. International Journal of Toxicology, 20(3), 161–3. [PubMed: 11488558]

Denton PW, & Garcia JV, (2009). Novel humanized mouse models for HIV research. Current HIV/AIDS Reports, 6(1), 13–19. [PubMed: 19149992]

Denton PW, Krisko JF, Powell DA, Mathias M, Kwak YT, Martinez-Torres F, Zou W, Payne DA, Estes JD, & Garcia JV, (2010). Systemic administration of antiretrovirals prior to exposure prevents rectal and intravenous HIV-1 transmission in humanized BLT mice. PLoS ONE, 5(1). Available from: https://journals.plos.org/plosone/article?id=10.1371/journal.pone.0008829 [Accessed 18 September 2018]

Edén A, Fuchs D, Hagberg L, Nilsson S, Spudich S, Svennerholm B, Price RW, & Gisslén M, (2010). HIV-1 viral escape in cerebrospinal fluid of subjects on suppressive antiretroviral treatment. The Journal of Infectious Diseases, 202(12), 1819–25. [PubMed: 21050119]

Farhadian S, Patel P, & Spudich S, (2017). Neurological complications of HIV infection. Current Infectious Disease Reports, 19(50). Available from: 10.1007/s11908-017-0606-5 [Epub ahead of print] [Accessed 19 September 2018]

Griffin L, Annaert P, & Brouwer KL, (2011). Influence of drug transport proteins on the pharmacokinetics and drug interactions of HIV protease inhibitors. Journal of Pharmaceutical Sciences, 100(9), 3636–54. [PubMed: 21698598]

Hassounah SA, Mesplède T, Quashie PK, Oliveira M, Sandstrom PA, & Wainberg MA, (2014). Effect of HIV-1 Integrase resistance mutations When introduced into SIVmac239 on susceptibility to integrase strand transfer inhibitors. Journal of Virology, 88(17), 9683–92. [PubMed: 24920794]

Hatziioannou T, & Evans DT, (2012). Animal models for HIV/AIDS research. Nature Reviews Microbiology, 10(12), 852–67. [PubMed: 23154262]

Hoefnagel JG, Koopmans PP, Burger DM, Schuurman R, & Galama JM, (2005). Role of the inhibitory quotient in HIV therapy. Antiviral Therapy, 10(8), 879–92. [PubMed: 16430193]

Ito K, Uchida Y, Ohtsuki S, Aizawa S, Kawakami H, Katsukura Y, Kamiie J, & Terasaki T, (2011). Quantitative membrane protein expression at the blood-brain barrier of adult and younger cynomolgus monkeys. Journal of Pharmaceutical Science, 100(9), 3939–50.

Joseph SB, Arrildt KT, Sturdevant CB, & Swanstrom R, (2014). HIV-1 target cells in the CNS. Journal of Neurovirology, 276–89. [PubMed: 25236812]

Letendre S, (2011). Central nervous system complications in HIV disease: HIV-associated neurocognitive disorder. Topics in Antiviral Medicine, 19(4), 137–42. [PubMed: 22156215]

Liu X, Smith BJ, Chen C, Callegari E, Becker SL, Chen X, Cianfrogna J, Doran AC, Doran SD, Gibbs JP, Hosea N, Liu J, Nelson FR, Szewc MA, & Van Deusen J, (2006). Evaluation of cerebrospinal fluid concentration and plasma free concentration as a surrogate measurement for brain free concentration. Drug Metabolism and Disposition, 34(9), 1443–7. [PubMed: 16760229]

MacArthur RD, & Novak RM, (2008). Reviews of anti-infective agents: maraviroc: the first of a new class of antiretroviral agents. Clinical Infectious Diseases, 47(2), 236–41. [PubMed: 18532888]

Marra CM, (2015). HIV-associated neurocognitive disorders and central nervous system drug penetration: what next? Antiviral Therapy, 20(4), 365–7. [PubMed: 25781980]

Martina T, (2013). Atazanavir causing CNS toxicity? Unexplained neurological symptoms in two patients recently started on atazanavir. Journal of AIDS & Clinical Research, 4(3), doi: 10.4172/2155-6113.1000196. Available from: https://www.omicsonline.org/atazanavir-causing-cns-toxicity-unexplained-neurological-symptoms-in-two-patients-recently-started-on-atazanavir-2155-6113.1000196.php?aid=12234 [Accessed 19 September 2018]

Mast N, Li Y, Linger M, Clark M, Wiseman J, & Pikuleva IA, (2014). Pharmacologic stimulation of Cytochrome P450 46A1 and cerebral cholesterol turnover in mice. Journal of Biological Chemistry, 289(6), 3529–38 [PubMed: 24352658]

Mathez D, Schinazi RF, Liotta DC, & Leibowitch J, (1993). Infectious amplification of wild-type human immunodeficiency virus from patients' lymphocytes and modulation by reverse transcriptase inhibitors in vitro. Antimicrobial Agents and Chemotherapy, 37(10), 2206–11. [PubMed: 7504908]

Mukerji SS, Misra V, Lorenz DR, Uno H, Morgello S, Franklin D, Ellis RJ, Letendre S, & Gabuzda D, (2018). Impact of antiretroviral regimens on CSF viral escape in a prospective multicohort study of ART-experienced HIV-1 infected adults in the United States. Clinical Infectious Diseases, Available from: 10.1093/cid/ciy267 [Epub ahead of print] [Accessed 1 September 2018]

Neff PC, Ndolo T, Tandon A, Habu Y, & Akkina R, (2010). Oral pre-exposure prophylaxis by anti-retrovirals raltegravir and maraviroc protects against HIV-1 vaginal transmission in a humanized mouse model. PLoS ONE, 5(12), Available from: https://journals.plos.org/plosone/article?id=10.1371/journal.pone.0015257 [Accessed 1 May 2018]

New DR, Maggirwar SB, Epstein LG, Dewhurst S, & Gelbard HS, (1998). HIV-1 Tat induces neuronal death via tumor necrosis factor-α and activation of non-N-methyl-D-aspartate receptors by a NFκB-independent mechanism. Journal of Biological Chemistry, 273(28), 17852–8. [PubMed: 9651389]

Nguyen A, Rossi S, Croteau D, Best BM, Clifford D, Collier AC, Gelman B, Marra C, McArthur J, McCutchan JA, Morgello S, Simpson D, Ellis RJ, Grant I, Capparelli E, & Letendre S; CHARTER Group, (2013). Etravirine in CSF is highly protein bound. Journal of Antimicrobial Chemotherapy, 68(5), 1161–8. [PubMed: 23335197]

Nicol M, Taylor J, Pastick K, Fisher J, Karuganda C, Rhein J, Williams DA, Meya D, Boulware D, & Lukande R (2018). Differential brain tissue penetration of antiretrovirals and fluconazole. In Conference on Retroviruses and Opportunistic Infections (CROI) 4–7 March, 2018 Boston, Massachusetts Abstract Number: 474. Available from: https://www.croiconference.org/sessions/differential-brain-tissue-penetration-antiretrovirals-and-fluconazole [Accessed 10 August 2018]

North TW, Van Rompay KK, Higgins J, Matthews TB, Wadford DA, Pedersen NC, & Schinazi RF, (2005). Suppression of virus load by highly active antiretroviral therapy in rhesus macaques infected with a recombinant simian immunodeficiency virus containing reverse transcriptase from human immunodeficiency virus Type 1. Journal of Virology, 79(12), 7349–54. [PubMed: 15919889]

North TW, Higgins J, Deere JD, Hayes TL, Villalobos A, Adamson L, Shacklett BL, Schinazi RF, & Luciw PA, (2010). Viral sanctuaries during highly active antiretroviral therapy in a nonhuman primate model for AIDS. Journal of Virology, 84(6), 2913–22. [PubMed: 20032180]

Pal R, Galmin L, Pereira LE, Li B, Zhang J, Li D, Francis J, McNicholl JM, Weiss DE, & Smith JM, (2012). Virological and molecular characterization of a simian human immunodeficiency virus (SHIV) encoding the envelope and reverse transcriptase genes from HIV-1. Virology, 432(1), 173–83. [PubMed: 22769870]

Rambeck B, Jürgens UH, May TW, Pannek HW, Behne F, Ebner A, Gorji A, Straub H, Speckmann EJ, Pohlmann-Eden B, & Löscher W, (2006). Comparison of brain extracellular fluid, brain tissue, cerebrospinal fluid, and serum concentrations of antiepileptic drugs measured intraoperatively in patients with intractable epilepsy. Epilepsia, 47(4), 681–94. [PubMed: 16650134]

Robertson K, Liner J, & Meeker RB, (2012). Antiretroviral neurotoxicity. Journal of Neurovirology, 18(5), 388–99. [PubMed: 22811264]

Robichaud G, Garrard KP, Barry JA, & Muddiman DC, (2013). MSiReader: An open-source interface to view and analyze high resolving power MS imaging files on matlab platform. Journal of the American Society for Mass Spectrometry, 24(5), 718–21. [PubMed: 23536269]

Shen DD, Artru AA, & Adkison KK, (2004). Principles and applicability of CSF sampling for the assessment of CNS drug delivery and pharmacodynamics. Advanced Drug Delivery Reviews, 56(12), 1825–57. [PubMed: 15381336]

Shytaj IL, Norelli S, Chirullo B, Della Corte A, Collins M, Yalley-Ogunro J, Greenhouse J, Iraci N, Acosta EP, Barreca ML, Lewis MG, & Savarino A, (2012). A highly intensified ART regimen induces long-term viral suppression and restriction of the viral reservoir in a simian AIDS model. PLoS Pathogens, 8(6). Available from: https://journals.plos.org/plospathogens/article?id=10.1371/journal.ppat.1002774 [Accessed 1 September 2018].

Smith DA, Di L, & Kerns EH, (2010). The effect of plasma protein binding on in vivo efficacy: misconceptions in drug discovery. Nature Reviews Drug Discovery, 9(12), 929–39. [PubMed: 21119731]

Srinivas N, Maffuid K, & Kashuba ADM, (2018). Clinical pharmacokinetics and pharmacodynamics of drugs in the central nervous system. Clinical Pharmacokinetics, 57(9), 1059–74. [PubMed: 29464550]

Strazielle N, & Ghersi-Egea JF, (2015). Efflux transporters in blood-brain interfaces of the developing brain. Frontiers in Neuroscience, Available from: 10.3389/fnins.2015.00021 [Accessed 7 October 2018].

Thompson CG, Bokhart MT, Sykes C, Adamson L, Fedoriw Y, Luciw PA, Muddiman DC, Kashuba AD, & Rosen EP, (2015). Mass spectrometry imaging reveals heterogeneous efavirenz distribution within putative HIV reservoirs. Antimicrobial Agents and Chemotherapy, 59(5), 2944–8. [PubMed: 25733502]

Thompson CG, Fallon JK, Mathews M, Charlins P, Remling-Mulder L, Kovarova M, Adamson L, Srinivas N, Schauer A, Sykes C, Luciw P, Garcia JV, Akkina R, Smith PC, & Kashuba ADM, (2017). Multimodal analysis of drug transporter expression in gastrointestinal tissue. AIDS, 31(12), 1669–78. [PubMed: 28590331]

Valcour V, Chalermchai T, Sailasuta N, Marovich M, Lerdlum S, Suttichom D, Suwanwela NC, Jagodzinski L, Michael N, Spudich S, van Griensven F, de Souza M, Kim J, & Ananworanich J; RV254/SEARCH 010 Study Group, (2012). Central nervous system viral invasion and inflammation during acute HIV infection. The Journal of Infectious Diseases, 206(2), 275–82. [PubMed: 22551810]

Van Rompay KK, Cherrington JM, Marthas ML, Berardi CJ, Mulato AS, Spinner A, Tarara RP, Canfield DR, Telm S, Bischofberger N, & Pedersen NC, (1996). 9- [2- (phosphonomethoxy) propyl] adenine therapy of established simian immunodeficiency virus infection in infant rhesus macaques. Antimicrobial Agents and Chemotherapy, 40(11), 2586–91. [PubMed: 8913470]

Weiss J, Rose J, Storch CH, Ketabi-Kiyanvash N, Sauer A, Haefeli WE, & Efferth T, (2007). Modulation of human BCRP (ABCG2) activity by anti-HIV drugs. Journal of Antimicrobial Chemotherapy, 59(2), 238–45. [PubMed: 17202245]

Wijnholds J, deLange EC, Scheffer GL, van den Berg DJ, Mol CA, van der Valk M, Schinkel AH, Scheper RJ, Breimer DD, & Borst P, (2000).Multidrug resistance protein 1 protects the choroid plexus epithelium and contributes to the blood-cerebrospinal fluid barrier. Journal of Clinical Investigation, 105(3):279–85. [PubMed: 10675353]

Winston A, & Khoo S, (2008). Clinical application of the inhibitory quotient: is there a role in HIV protease inhibitor therapy? Current Opinion in HIV and AIDS, 3(6), 608–11 [PubMed: 19373031]

Witrouw M, Pannecouque C, Switzer WM, Folks TM, De Clercq E, & Heneine W, (2004). Susceptibility of HIV-2, SIV and SHIV to various anti-HIV-1 compounds: implications for treatment and postexposure prophylaxis. Antiviral Therapy, 9(1), 57–65. [PubMed: 15040537]

Yilmaz A, Price RW, & Gisslén M, (2012). Antiretroviral drug treatment of CNS HIV-1 infection. Journal of Antimicrobial Chemotherapy, 67(2), 299–311. [PubMed: 22160207]

Zayyad Z, & Spudich S, (2015). Neuropathogenesis of HIV: from initial neuroinvasion to HIV-associated neurocognitive disorder (HAND). Current HIV/AIDS Reports, 12(1), 16–24. [PubMed: 25604237]

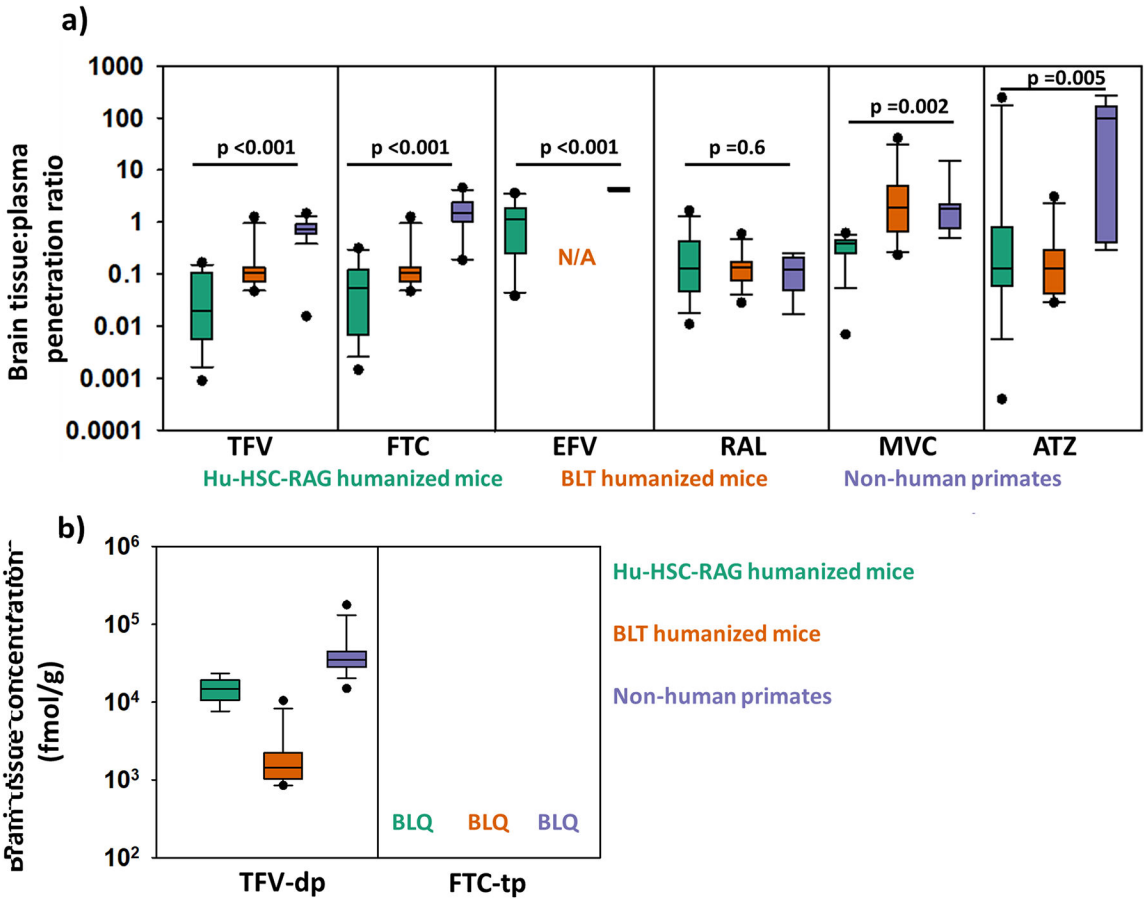

Figure 1.

a) Antiretroviral brain tissue:plasma penetration ratio in humanized-mice and nonhuman primates.

Only the brain tissue:plasma penetration ratio of RAL was preserved across all three species (p=0.6). MVC penetration did not differ between the BLT mice and nonhuman primates (p=1.0) and ATZ penetration did not differ between the hu-HSC-RAG and BLT mice (p=0.8). For all other ARVs, the order of brain tissue penetration ratio was NHP>BLT>hu-HSC-RAG. Boxes represent 1st and 3rd quartile with median line. Whiskers represent 10th and 90th percentile and filled circles represent outliers. The BLT mice were not dosed with EFV due to toxicity issues.

b) Concentration of active metabolites of tenofovir and emtricitabine in the brain tissue of humanized mice and nonhuman primates.

FTC-tp was not detected in the brain tissue of any of the animal models. Median brain tissue concentrations of tenofovir diphosphate (TFV-dp) were 10-fold higher in the hu-HSC-RAG mice compared to the BLT mice (14371 fmol/g vs 1443 fmol/g, p=0.29). TFV-dp concentration in the NHP brain was 34840 fmol/g.

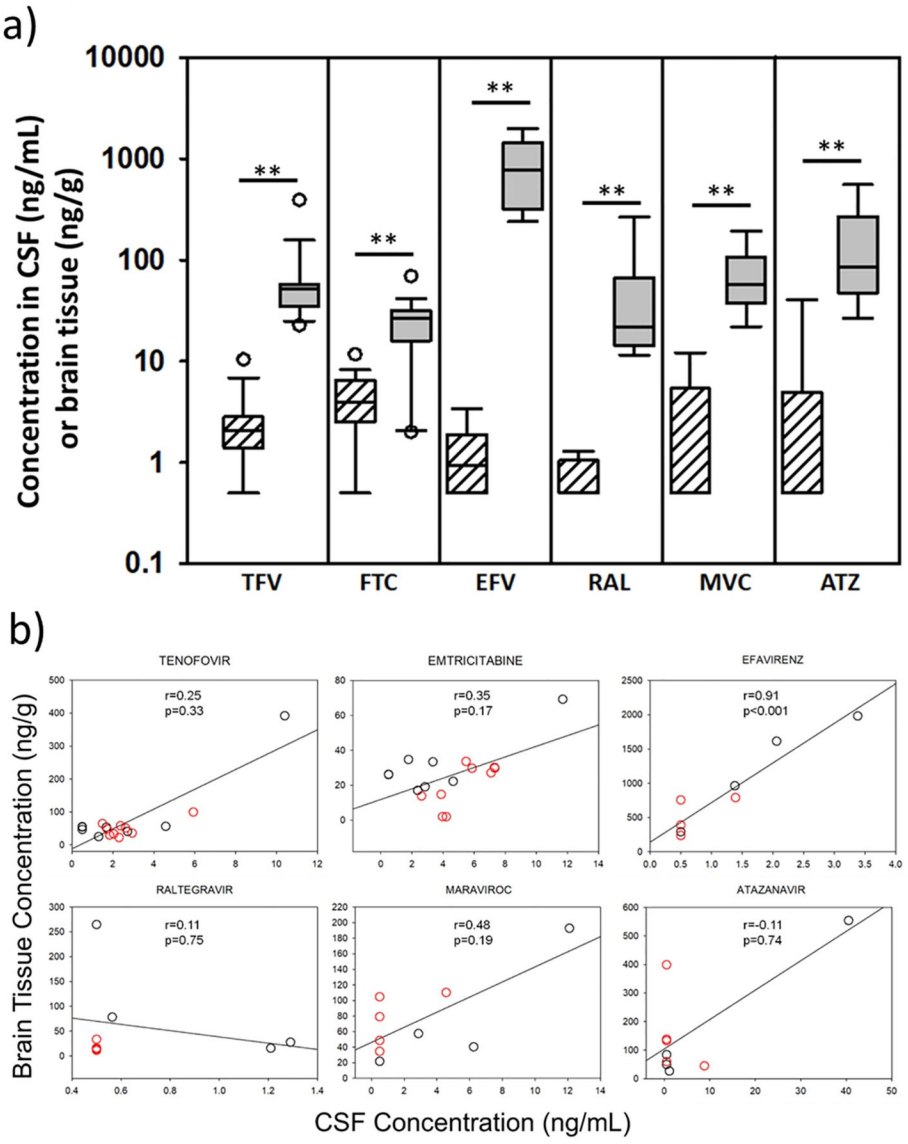

Figure 2.

a) Antiretroviral concentrations in the CSF and brain tissue of nonhuman primates.

ARV concentrations are shown in the CSF (stripes) and brain tissue (solid fill) of NHPs. Brain tissue concentrations were higher than CSF for all ARVs ($p<0.001$). Boxes represent 1st and 3rd quartile with median line. Whiskers represent 10th and 90th percentile. Open circles represent outliers.

b) Correlation analysis between antiretroviral concentrations in the brain tissue and cerebrospinal fluid in rhesus macaques.

Significant correlation between brain tissue and CSF concentration was only noted for efavirenz ($r=0.91$; $p<0.001$). Black open circles – uninfected animals and red open circles – RT-SHIV-infected animals. Legend: CSF – cerebrospinal fluid.

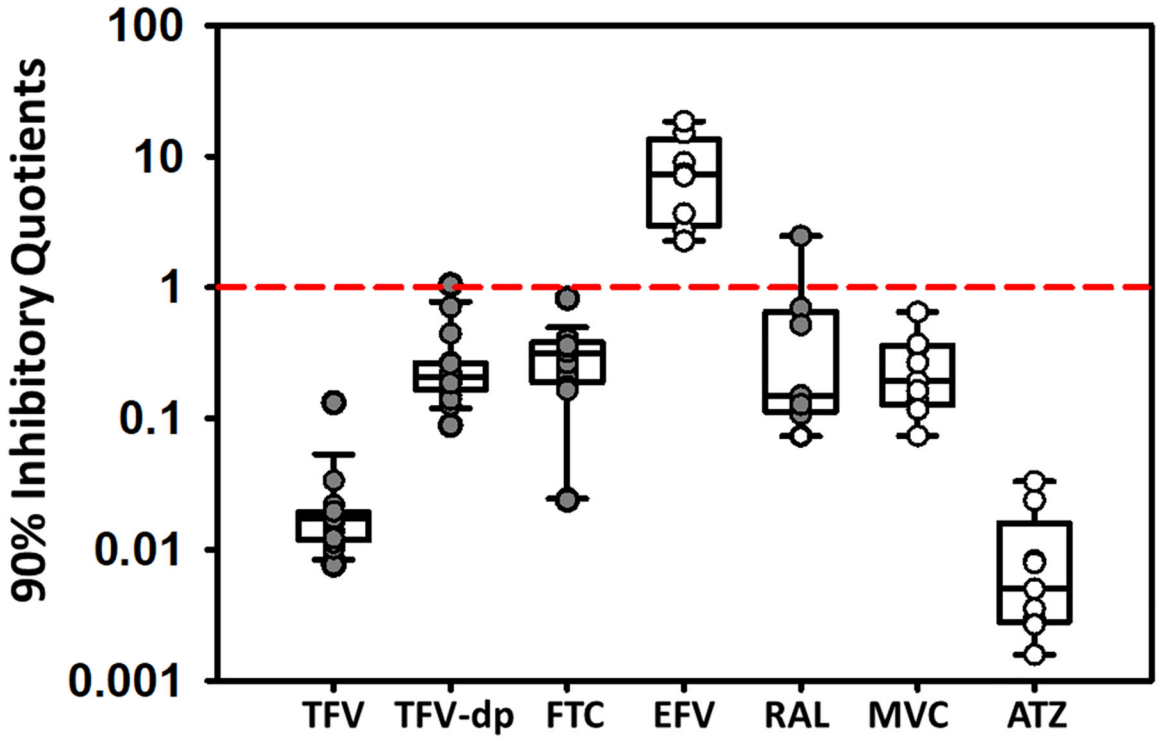

Figure 3.

90% inhibitory quotients for antiretrovirals and metabolites in the brain tissue of nonhuman primates.

EFV had the highest IQ_{90} values in the nonhuman primates, which was above 1 for all 8 animals. In case of TFV, TFV-dp, FTC, MVC, and ATZ none of the animals had IQ_{90} above 1. Boxes represent 1st and 3rd quartile with median line. Whiskers represent 10th and 90th percentile. Dot-plot overlay represents individual values; open circles represent values that were derived from the unbound brain tissue concentrations while the grey filled circles represent values that derived from the total brain tissue concentrations.

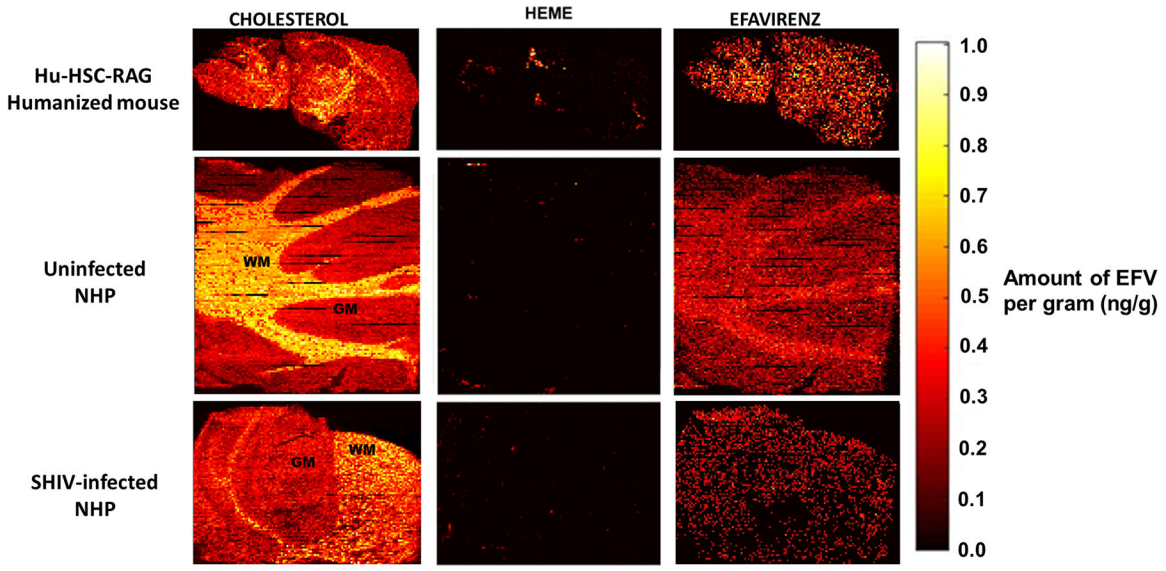

Figure 4.

Mass-spectrometry imaging of cholesterol and the amount of efavirenz per volumetric pixel in the brain tissue of preclinical species.

The cholesterol heat maps shown on the left-pane are used to indicate morphological differences in the brain tissue between the white matter and the grey matter. The heme distribution maps shown in the middle-pane were used as a marker of blood contamination in the brain tissue samples. The efavirenz heat maps shown on the right-pane are masked with the heme distribution maps to show efavirenz response outside of the blood contamination. The efavirenz distribution maps are scaled to the total ng/g concentration of efavirenz per volumetric pixel.

(a) In the humanized mice, efavirenz distribution was detected in only one infected hu-HSC-RAG mouse, but was distributed homogeneously throughout the brain tissue. The heme distribution in this animal indicated that there was some blood contamination which accounted for 30% of the total efavirenz response in the brain tissue (b) In the cerebellum tissue of uninfected NHPs, clear preferential distribution of efavirenz was noted in the white matter compared to the grey matter. Heme distribution in the uninfected NHPs was minimal, accounting for ~1% of the total efavirenz response (c) In the RT-SHIV-infected animals, 86% lower concentrations of efavirenz was detected in the brain tissue, which made detection of distribution differences more challenging. Heme distribution in the RT-SHIV-infected NHPs was minimal, accounting for ~1% of the total efavirenz response. Legend: WM – white matter, GM – grey matter, NHP – nonhuman primate.

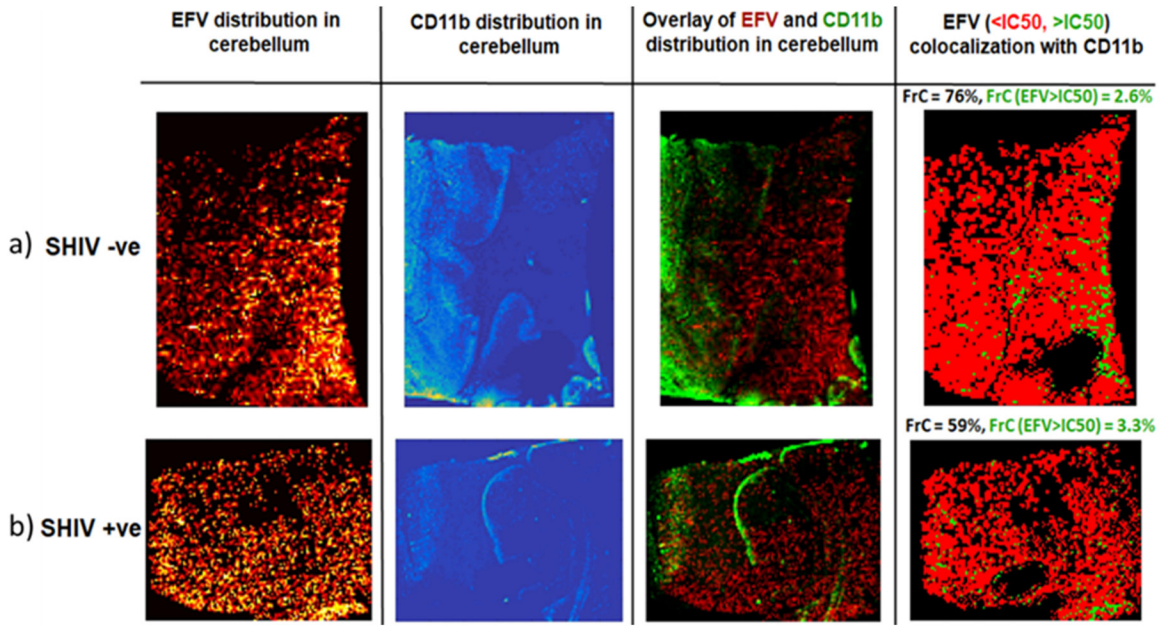

Figure 5.

Overlay between efavirenz MSI and CD11b+ cell distribution in the cerebellum tissue in (a) uninfected and (b) RT-SHIV-infected animals.

Distribution of EFV and CD11b+ cells in the cerebellum and the overlay of distribution are shown in (a) uninfected and (b) RT-SHIV-infected animals. In the far-left panel, brighter colours represent higher concentration of EFV. In the panel second from the left, light colour represents greater density of cells, increasing form light blue to yellow. In the panel second from the right, overlay between EFV MSI and cell distribution is shown. In far-right panel, only the target cells containing detectable EFV or EFV above IC_{50} are shown. Fractional coverage of the CD11b+ cells with detectable EFV was higher in the uninfected animals compared to the RT-SHIV infected animals. Coverage with EFV concentration $>IC_{50}$ was only 3% regardless of infection status.